Quantum wells in polar-nonpolar oxide heterojunction systems

C.-C Joseph Wang,[1,*] Bhagawan Sahu,[2] Hongki Min,[1] Wei-Cheng Lee,[1] and Allan H. MacDonald[1]
[1]*Department of Physics, The University of Texas at Austin, Austin, Texas 78712-0264, USA*
[2]*Microelectronics Research Center, The University of Texas at Austin, Austin, Texas 78758, USA*
(Received 5 October 2008; published 9 March 2009)

We address the electronic structure of quantum wells in polar-nonpolar oxide heterojunction systems focusing on the case of nonpolar $BaVO_3$ wells surrounded by polar $LaTiO_3$ barriers. Our discussion is based on a density-functional description using the local spin-density approximation with local-correlation corrections (LSDA+U). We conclude that a variety of quite different two-dimensional electron systems can occur at interfaces between insulating materials depending on band lineups and on the geometrical arrangement of polarity discontinuities.

DOI: 10.1103/PhysRevB.79.115408 PACS number(s): 73.20.−r, 73.21.Cd, 75.70.−i

I. INTRODUCTION

Complex oxide materials exhibit a wide variety of exotic phenomena from high-temperature superconductivity[1] to colossal magnetoresistance,[2] to electronic and orbital order.[3] Recently, inspired by advances in epitaxial growth techniques, there has been increasing interest[4–10] in making progress toward the goal of controlling oxide properties by designing layered structures at the atomic level. The class of artificial materials which has been studied most extensively is ABO_3 perovskites. Already there is evidence for the emergence of superconductivity from nonsuperconducting materials[5] and magnetism from nonmagnetic materials.[6] One element which distinguishes oxide heterojunction systems from weakly correlated semiconductor heterojunctions is the possibility of exploiting gradients in polarity[11] to help control electronic properties. In this article we study the electronic properties of oxide quantum wells in which the barrier and well materials have very different polarities, using the case of nonpolar $BaVO_3$ (BVO) wells surrounded by polar $LaTiO_3$ (LTO) barriers as an example.

Our paper is organized as follows. In Sec. II, we present a qualitative discussion of four possible polar-nonpolar quantum-well geometries. We have tested conjectures made in Sec. II by performing local spin-density approximation with local-correlation corrections (LSDA+U) calculations for BVO quantum wells in LTO and LTO quantum wells in BVO. Throughout this paper, we use LTO as shorthand for the perovskites associated with LaO and TiO_2 layers and BVO as shorthand for the perovskites associated with BaO and VO_2 layers. In Sec. III, we briefly detail the LSDA+U electronic structure calculation methods we have employed to model LTO/BVO/LTO or BVO/LTO/BVO quantum-well systems. The combination (LTO/BVO) was chosen because LTO is polar while BVO is not and because this material combination should not lead to large strains at the interface. Partly for convenience and partly because multiquantum-well systems are likely to be of equal experimental interest, we assume periodically repeated quantum wells so that we have a superlattice in the growth direction. In bulk both LTO and BVO are d^1 Mott insulators. We focus on heterojunction systems composed of materials which have the same d-band occupancies in the bulk because more possibilities exist for interface electronic structure compared to the case of heterojunctions between d^1 and d^0 materials such as $LaTiO_3/SrTiO_3$ for which interface metallicity appears to be inevitable. In Sec. IV we present the results of our *ab initio* electronic structure calculations for the two representative quantum-well systems and compare with the conjectures we made in Sec. II. Finally in Sec. V we briefly summarize our results.

II. POLAR-NONPOLAR QUANTUM-WELL STRUCTURES

In this section, we discuss four different possible geometries for a polar-nonpolar quantum-well system. The main points we wish to make are shown in Fig. 1 which illustrates approximate charge transfers and electric potentials. Throughout this discussion we use LTO to represent a prototypical d^1 polar perovskite and BVO to represent a prototypical d^1 nonpolar perovskite. We identify two possible geometries for both LTO/BVO/LTO [case (a) and case (c)] and BVO/LTO/BVO [case (b) and case (d)] quantum-well systems. At an interface between two strongly correlated bulk materials we should expect a complex interplay among the ionic potential energy, kinetic energy, and correlation energies of the two materials. By using density-functional theory with local correlations (LSDA+U), we can take into account those energies approximately with a single electron picture. The electronic structure is characterized most crudely by an ionic electron counting picture which neglects hybridization between oxygen and transition-metal orbitals and ignores the finite thickness of the various atomic layers. Using this picture, the $La^{+3}O^{-2}$ planes in LTO are positively charged and the $Ti^{+3}O_2^{-4}$ are negatively charged. In bulk BVO on the other hand, the $Ba^{+2}O^{-2}$ and $V^{+4}O_2^{-4}$ planes are neutral in the bulk. The transition-metal ions in both materials then have one electron in the d orbitals to maintain charge neutrality. When we combine polar perovskites with nonpolar ones, the transition-metal layer will distribute the d charges in a different way to compensate for the nonuniform distribution of ionized layers in this system, as illustrated in Fig. 1. The distributions labeled *ideal conjecture* in this figure assign the charge deficiency or excess to the two transition-metal layers adjacent to the quantum well, whereas the distributions labeled *realistic conjecture* assume additional charge redistri-

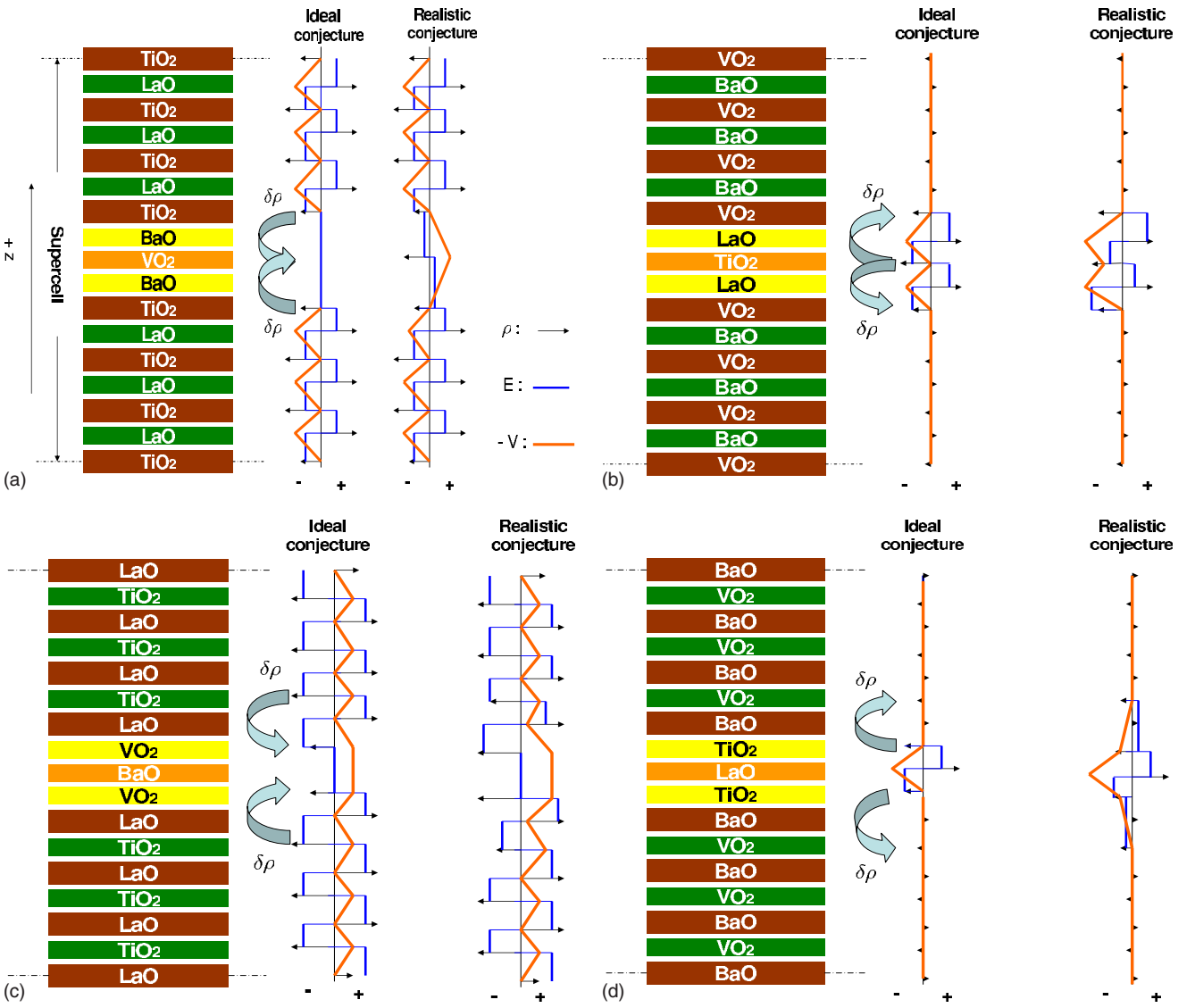

FIG. 1. (Color online) Approximate charge density, electric field, and electric potential distributions in different polar-nonpolar quantum-well systems with inversion symmetry in the quantum-well center. The arrows (black on line) indicate the expected charge densities ρ centered on different atomic layers; the piecewise constant thick lines (blue on line) indicate the expected electric fields E between the atomic layers; and the cusped lines (red on line) indicate the expected electric potential $-V(z)$ distribution. The signs + and − stand for the direction of electric field E, the value for ρ, and the potential $-V(z)$.

bution $\delta\rho$ due to the difference between V and Ti d-orbital energies. We discuss only cases in which the center of the quantum well is a center of inversion symmetry. In each case the number of layers which would have a positive charge in a bulk polar crystal differs from the number of layers which would have a negative charge.

In case (a), we have two BaO layers and one VO_2 layer inserted in the unit cell of a superlattice with six LaO^+ layers but seven TiO_2 layers. The charges in the supercell cannot be neutral if we assume that each TiO_2 is negatively charged as in the bulk LTO states. Instead, we expect that the extra electrons will be distributed evenly among the TiO_2 layers near the central VO_2 layer. The easiest way to accomplish this is to have the TiO_2 layers next to BaO layers to be $Ti^{+3.5}O_2^{-4}$ rather than $Ti^{+3}O_2^{-4}$, i.e., that they contain 0.5 d electrons per Ti rather than 1.0 d electrons per titanium. This idealized conjecture ignores d-p hybridization as well as the difference between the d-orbital energies on Ti and V sites. In particular a V^{+4} ion should have a lower intrinsic atomic levels than the Ti^{+3} ion. We should expect that charges might react locally to this difference by transferring additional electrons $\delta\rho$ to the VO_2 well from nearby TiO_2 layers. This additional charge transfer partially screens the original atomic energy level difference. These considerations are illustrated schematically in Fig. 1. The d-electron system electronic structure reconstructs in this way near the interface in reaction to the electrostatic potentials produced by the bulk crystal layer polarizations. Qualitatively similar considerations would apply to wider BVO quantum wells.

In case (b), we have two LaO^+ layers and one TiO_2 barrier layer in the middle of the supercell. By the same arguments as case (a), the simplest conjecture is that the VO_2 layers

nearest the TiO_2 layers will be negatively charged ($V^{+3.5}O_2^{-4}$) to keep the system neutral. The charge configuration $Ti^{+3}O_2^{-4}$ is maintained by the protection of two surrounding LaO^+ layers. Therefore, there will be 1.5 *d* electrons on V sites in the $V^{+3.5}O_2^{-4}$ layers and 9 *d* electrons in the supercell. However, the local physics is different in this case. The electron can respond locally by transferring electrons from the barrier TiO_2 to the VO_2 well layers. The reconstructed potential should therefore be lower in the well region in this case.

In case (c), we switch the ordering of layers from case (a) ($BaO \leftrightarrow VO_2$ and $LaO \leftrightarrow TiO_2$). There are seven positive-charged LaO^+ layers and six $Ti^{+3}O_2^{-4}$ layers. To compensate for the charge difference, VO_2 layers have to be negatively charged as $V^{+3.5}O_2^{-4}$ in the idealized conjecture illustrated. Additional charges can transfer from adjacent $Ti^{+3}O_2^{-4}$ to the $V^{+3.5}O_2^{-4}$ layers. The reconstructed potential should therefore be higher in the well region.

Similarly in case (d), the structure has been changed from case (b) by switching the ordering $BaO \leftrightarrow VO_2$ and $LaO \leftrightarrow TiO_2$. There is only one LaO^+ layer in this case. The abutting TiO_2 layers should have the configuration $Ti^{+3.5}O_2^{-4}$ to keep charge neutrality, resulting in a lower reconstructed local potential in the center of the cell. Notice that the magnitude of the additional charge transfer and its spatial distribution expected in the realistic pictures needs to be determined by self-consistent microscopic calculations. In Sec. III, we will focus on cases (a) and (b) to check the degree to which the qualitative pictures explained here agrees with the results of microscopic DFT calculations and to obtain further insight into the nature of the two-dimensional electron systems which these electronic reconstructions enforce. To avoid confusion to the readers, in microscopic calculation, the *d* electrons should be interpreted as the electrons occupying the bands, which hybridized with *s* and *p* orbitals, with dominant *d* character at transition-metal sites.

III. ELECTRONIC STRUCTURE CALCULATIONS

In our *ab initio* electronic structure calculations we have considered symmetric quantum-well geometries only, use the experimental atom positions[12,13] for LTO, and neglect atomic relaxation in the BVO layers. (The room-temperature crystal structure of BVO is not known experimentally.) The electronic structure calculations were performed using DFT with LSDA+*U* as implemented in the software package VASP.[14–16] Projector-augmented wave (PAW) pseudopotentials[17] are used to describe the electron-ion interaction. We sample the full superlattice Brillouin zone (BZ) with a $5\times5\times3$ mesh and used an energy cutoff of 410 eV which we found to be sufficient to reproduce bulk LTO properties. We used PAW pseudopotentials supplied by the VASP code for La, O, Ba, Ti, and V; but for Ba, Ti, and V, we used the one with semicore states treated as valence states. The screened local correlation *U* in the partially filled *d* bands of the transition-metal elements was treated using the rotationally invariant LSDA+*U* method due to Dudarev *et al.*[18] Since the La *f* bands lie much higher in energy in experiments[8,19] we impose a much larger $U_{La}=11$ eV on La *f* states to prevent their mixing with *d* bands at low energy. We chose $U_{Ti}=3.2$ eV and $J_{Ti}=0.9$ eV since these values reproduce the Mott-insulating nature of bulk LTO,[20] and we take U_V and J_V to be the same as U_{Ti} and J_{Ti}. We have varied U_V to check the robustness of our calculations and find that our conclusions are independent of this LSDA+*U* parameter.

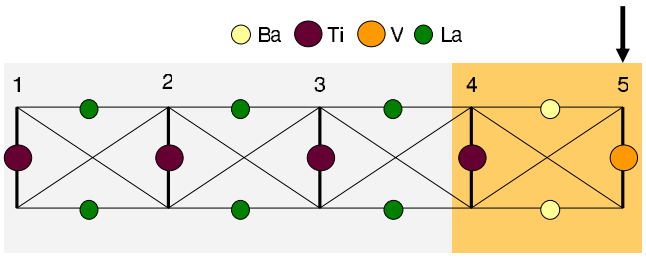

FIG. 2. (Color online) Half of the inversion symmetric unit cell. The quantum well consists of two layers of BaO and a monolayer of VO_2 and is embedded in bulk $LaTiO_3$. The light-orange shadowed region indicating the narrow active region in which the electronic interface reconstruction (EIR) driven by the polar discontinuity takes place. Oxygen atoms are located at the intersections of the checkered lines and form octahedra around the Ti and V atoms. The numbers specify labels for different layers. The downward arrow indicates the location of the VO_2 inversion plane.

IV. LSDA+*U* QUANTUM-WELL ELECTRONIC STRUCTURE

A. Case A: $(LaTiO_3)_3/(BaO)_2VO_2/(LaTiO_3)_3TiO_2$

The unit cell of the superlattice consists of a single VO_2 layer at the center of the well surrounded by two BaO layers as illustrated in Fig. 2. Because of the smaller *p*-*d* energy separation in bulk BVO compared to LTO, this material combination should form a quantum well centered on the VO_2 layer, assuming that the *p* bands of the two materials are nearly aligned at the interface. In our superlattice the BVO quantum-well layers are separated by seven TiO_2 transition-metal layers, each in turn separated by a LaO layer. Half of the inversion symmetric unit cell is shown in Fig. 2 in which the VO_2 inversion plane is marked by an arrow. Ti and V in bulk LTO and BVO, respectively, both have nominal valence charge d^1. In the quantum-well structure we study here the number of LaO layers, which are positively charged in the polar LTO crystal, is one smaller than the number of TiO_2 layers. It follows that the total *d* charge per transition metal summed over all layers is expected to be reduced by one. Unless the inversion symmetry is broken we should expect the missing *d* charge to be symmetrically distributed around the quantum-well center. The simplified assumptions of Sec. II would divide this valence change between the two TiO_2 layers adjacent to the quantum well.

Figure 3 shows the *d*-projected DOS at a Ti site and a V site in each TiO_2 and VO_2 plane. The states below −1.5 eV are the *d*-*p* bonding states between Ti and V atoms and their neighboring oxygens which have dominant *p* character, whereas the states near the Fermi level ($E=E_F$) are the antibonding states which have dominant *d* character. As we move through the superlattice from TO_2 barrier layers to the

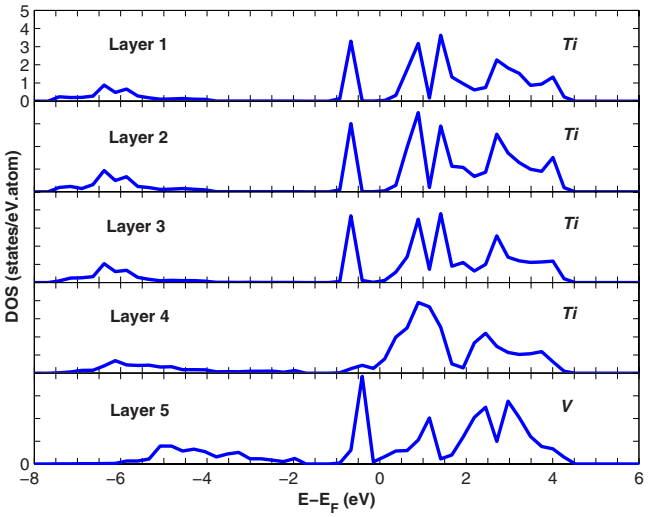

FIG. 3. (Color online) Layer-resolved *d*-projected density of states (DOS) at Ti and V sites versus energy. The layer labeling is defined in Fig. 2.

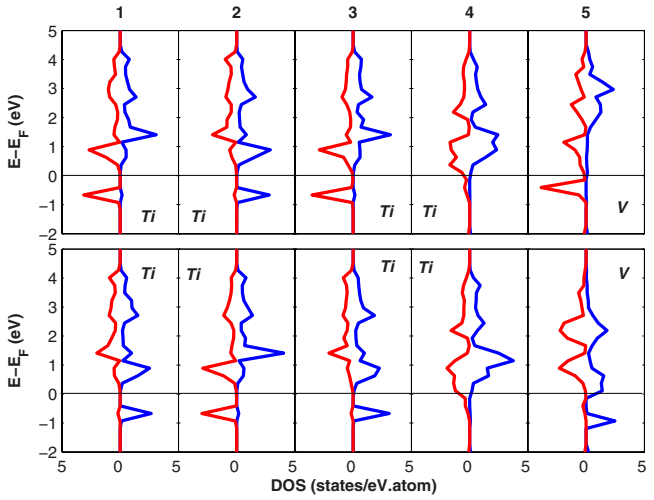

FIG. 4. (Color online) Spin and layer resolved densities of states versus energy. The labels on top are layer labels as in Fig. 2. Since we allow *G*-type antifferomagnetic (AFM) order in the barrier material, there are two distinct transition-metal atoms in each layer. The DOS for majority spins and minority spins are represented by red and blue lines, respectively, and the Fermi level is marked with a horizontal dark line at $E=E_F$.

VO_2 we see the DOS evolve from the typical bulk LTO form (layers 1 to 3) to a form near the heterojunction. In particular, there is a large depletion away from atomiclike d^1 charges in layer 4. The electronic reconstruction which accommodates the band offsets and the polarity discontinuity is evidently very strongly in layers 4 and 6 surrounding quantum-well layer 5 (layer 6 is not shown in Fig. 3 to avoid redundancies because of the inversion symmetry of the system). We also observe that the *p*-*d* separation is maintained at the VO_2 layer as expected after the electronic reconstruction. The total electron transfer from layer 4 is larger than in the ideal conjecture, as expected, and more remote layers participate in the transfer because of oxygen mediated coherence between transition-metal orbitals centered on different layers.

Most Mott insulators are orbitally and magnetically ordered. In order to gain some insight into the way in which the magnetic order is disturbed by the quantum-well structure, we plot in Fig. 4 the spin-resolved *d*-projected DOS in all layers. In our calculations we find *G*-type AFM order in which neighboring transition metals ions have opposite spins both within and between layers for the bulklike TiO_2 layers. (layers 1, 2, and 3 in Fig. 4). Layer 4 on the other hand has an overall magnetic moment of around $0.1\mu_B$ per Ti ion indicating a ferromagnetic layer. Because of the EIR, the magnetic order in the VO_2 plane changes from AFM to ferromagnetic. The projected moments on each Ti ions in the AFM bulklike TiO_2 layers are calculated to be $0.74\mu_B$ inside the Ti ionic radius which is fixed in our calculation by the pseudopotential construction. We believe that by enlarging the Ti ionic radius, we can get *d*-orbital integrated moments close to the $1\mu_B$ value expected for d^1 Mott insulators. Note that ferromagnetism is induced in the VO_2 layer by the two adjacent strongly depopulated and ferromagnetic TiO_2 layers.

Figure 5 shows the superlattice band structure along high-symmetry directions in the Brillouin zone. The bands [five majority (red) spin bands and five minority (blue) spin bands], which lie far below the E_F (in the energy range between −1 and −0.6 eV), can be identified as bulk LTO *d*-charge character bands by comparing with Fig. 4 and calculating band-decomposed local charge density contributions. In the supercell, we have five bulk TiO_2 layers (layers 1, 2, 3, 7, and 8) in our superlattice corresponding in the antiferromagnetic state to ten full bands (five spin up and five spin down). Therefore, there should be ten full bulklike

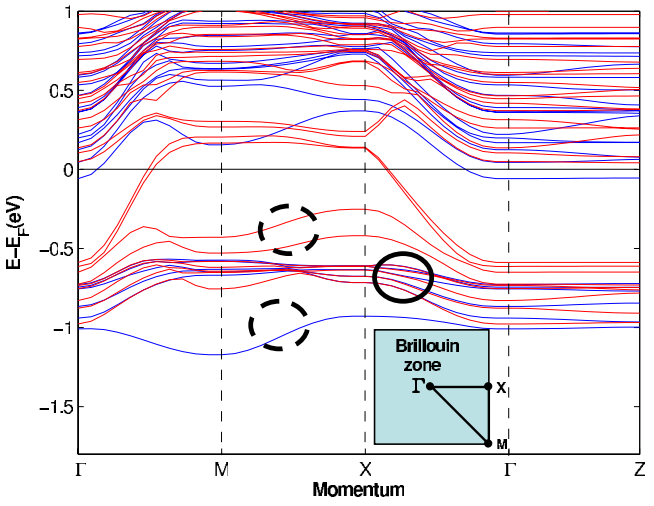

FIG. 5. (Color online) Spin-resolved band structure at the Brillouin zone. The horizontal axis represents superlattice crystal momentum. The red solid lines represents the majority-spin bands, and the blue ones are the minority-spin bands. The momentum dependence along the layer direction k_z is indicated in the region between the Γ and *Z* points. The full circle marks the d^1 bands for Ti atoms in LTO bulk states. The dashed circles represents the *d* bands for V atoms in VO_2. The bands associated with EIR are flat along k_z demonstrating their quasi-two-dimensional character. The shadowed blue square represents the projection of the superlattice Brillouin zone in the plane of the quantum well.

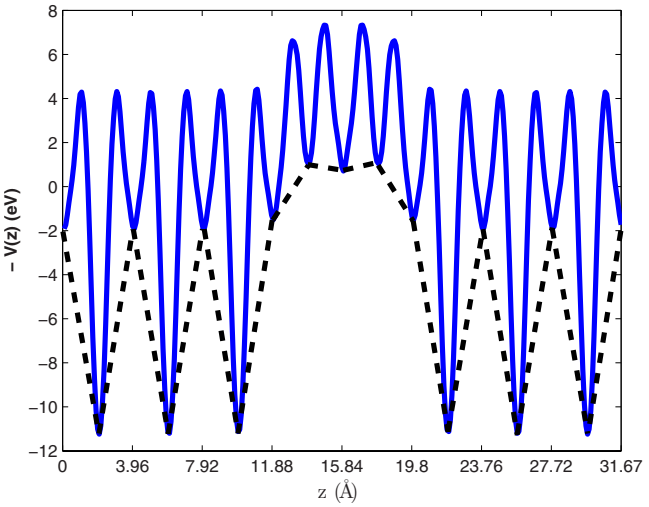

FIG. 6. (Color online) Plane-averaged Hartree potential along the layer-growth direction z. The blue curve represents the Hartree potential experienced by electrons $-eV(z)$. The dashed line indicates the net potential variation between charge-concentration centers in each layer.

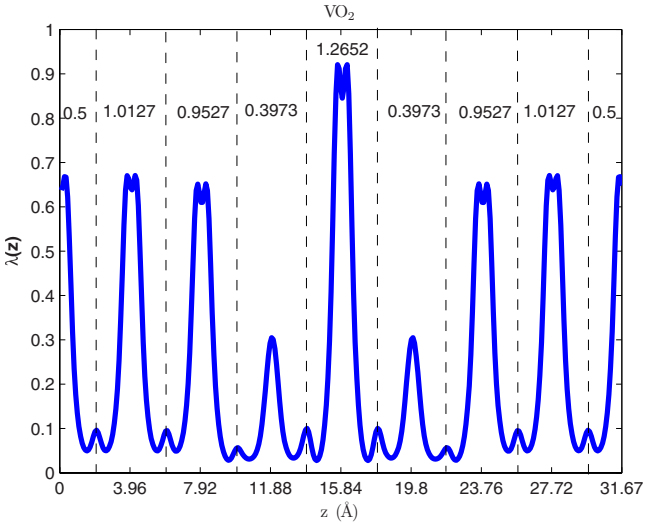

FIG. 7. (Color online) Linear electron number density $\lambda(z)$ along layer-growth direction z. The dashed lines represent the boundaries used for the partitioning of density into contributions from different layers. The total number of electrons in each layer contributed by the d-character bands in Fig. 5 is indicated by the numerical values between dashed lines. In this case, the total number of electrons in the supercell is seven.

LTO d bands, identified by the solid circle, in Fig. 5. Two full majority-spin bands and one full minority-spin band (near −1 eV) highlighted by two dashed circles are associated with the d charges in the VO_2 layers. The two majority bands close to the interface states in energy and are hybridized along the layer-growth direction and delocalized (this interpretation has been verified by separating the charge density contribution of those bands). Because of this hybridization, the total d charges (2.4053 e^-) at the V sites are smaller than the 3 e^- value which would be implied by a local interpretation of the band structure. It can in general be misleading to estimate the number of charges at transition-metal ions by counting the number of reconstructed bands with a particular dominant orbital character. The three partially full bands (one minority band and two majority bands) near the Fermi surface E_F are the bands responsible for the charge depletion at the TiO_2 layers adjacent to the quantum well (layers 4 and 6). The momentum k_z dependence of the electronic states is shown on the right panel of Fig. 5 [from momentum (0, 0, 0) at Γ to $(0,0,k_z)$ at Z]. It shows that the states at the Fermi energy form a two-dimensional electron gas centered on three layers, the active region. Notice that there also appears a flat band between M and X, which corresponds to the direction away from the bonding direction between Ti and O atoms in charge depleting the TiO_2 layers, due to the fact there is negligible tunneling of electrons along this direction. The two-dimensional system is metallic in this case and has three partially filled bands.

Since we have discussed the local potential for the electron in case (a) in Fig. 1 based on qualitative model in which we assume the charges at each layer are concentrated in a single layer along the layer direction, we would like to examine how the crude model prediction compares with actual DFT predictions. In Fig. 6, the DFT plane-averaged Hartree potential for the electrons is shown. First TiO_2 layer starts at $z=0$ and layers repeat with a spatial period of 3.96 Å and with the central layer ($z=15.84$ Å) of the supercell substituted by the VO_2 layer. First LaO layer is located at $z=1.98$ Å and these layers repeat with a period of 3.96 Å except that the two layers surrounding the central VO_2 layer correspond instead to BaO layers. By inspecting the variation of the local minima in the potential, we can see that the qualitative behavior anticipated in case (a) in Fig. 1 is valid, as shown by the black-dashed line. The electric field in the qualitative model should be considered as a macroscopically averaged electric field between potential minima in the microscopic calculations. Notice that the potential of the VO_2 layer is somewhat lower than anticipated.

In Fig. 7, we show the linear electron number density $\lambda(z) \equiv 0.5 \int \rho(x,y,z) dxdy$ along the layer-growth direction. The charge number spatial distribution $\rho(x,y,z)$ is normalized per transverse unit cell which is doubled because of the system's antiferromagnetic order and includes the total number of electrons contributed by the d bands between with energies up to 1.5 eV below the Fermi level. (See Fig. 5.) Factor 0.5 is used to convert the normalization to d electrons per transition-metal ion to facilitate comparison with the qualitative picture. The dashed lines represent the boundaries for the transition-metal oxide layers used in this electron number construction. The area under the curve $\lambda(z)$ represents the total number of electrons from all d bands. We see an apparent charge depletion at the TiO_2 layers centered at $z=11.88$ Å and $z=19.8$ Å along with large charge accumulation at the VO_2 layer. There is only minor charge depletion at second-nearest TiO_2 layers ($z=7.92$ Å and $z=23.76$ Å) away from VO_2 layer. The total charges from the d bands, 7 e^-, are obtained by adding the number of electrons at each layers and agree with the qualitative predictions for case (a). The number of electrons in the depleted TiO_2 layers is 0.3793. The other layers have small deviation from one elec-

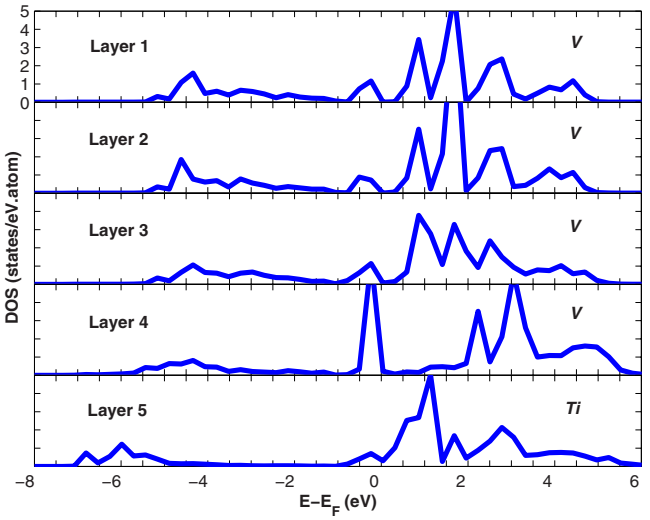

FIG. 8. (Color online) Layer-resolved *d*-projected density of states at Ti and V sites versus energy.

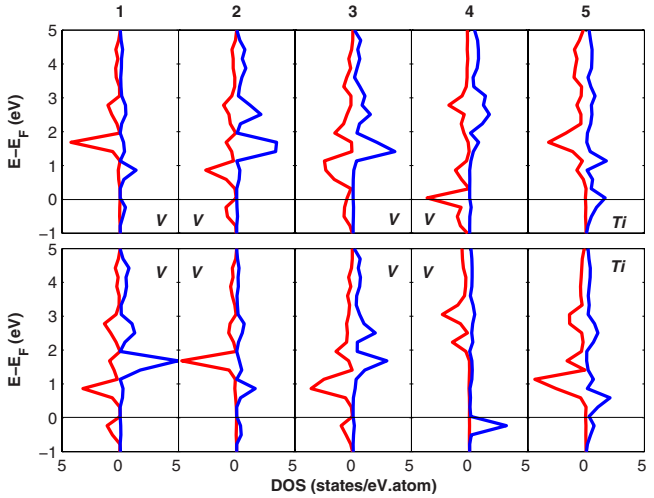

FIG. 9. (Color online) Spin and layer resolved densities of states versus energy. The labels on top are the layer labels indicated in Fig. 2. Since we allow *G*-type AFM order in the barrier material, there are two distinct transition-metal ions in each layer. The DOS for majority spins and minority spins are represented by red and blue lines, respectively.

tron. The calculation shows a clear deviation from ideal conjecture we made for this case and is closer to the realistic conjecture. In general, the charges in the well are mainly transferred from the adjacent TiO_2 layers, but there is also a minor contribution from other TiO_2 layers as shown from the number of electrons in each layer.

B. Case B: $(BaVO_3)_3/(LaO)_2TiO_2/(BaVO_3)_3VO_2$

In this section, we consider the quantum-well structure shown in case (b). In this case, the number of LaO layers, which are positively charged in the polar LTO crystal, is greater than the number of TiO_2 layer by one. It follows that the total *d* electrons per transition metal summed over all layers are expected to be increased by one. Unless the inversion symmetry is broken we should expect the extra *d* charge to be symmetrically distributed around the quantum-well center.

Figure 8 shows the *d*-projected DOS at a Ti site and a V site in each TO_2 and VO_2 plane. The states below −1 eV are the *p*-*d*-bonding states between the transition-metal atoms (Ti and V) and the *p* orbitals of the neighboring oxygens and have dominant *p* character. The states near the Fermi level ($E=E_F$), on the other hand, have dominant *d* character. As we move through the superlattice from the VO_2 layers to the TiO_2 barrier layer, we see the DOS evolve from the typical bulk BVO layer form (layers 1 to 3) to a form near the heterojunction. In particular, we see a strong peak in DOS in layer 4 near the Fermi energy E_F with 1.6 e^- per V ion in agreement with our conjectures. As far as magnetic order is concerned (Fig. 9), we find *G*-type AFM order in which neighboring transition metals ions have opposite spins both within and between layers for the bulklike VO_2 layers (layers 1 and 2). The magnetic orders in layers 3 and 5 are reconstructed to be ferromagnetic with the magnetic moment $0.9755\mu_B$ per V ion and the moment $0.4750\mu_B$ per Ti, respectively. The magnetic order in layer 4 is ferrimagnetic with a net magnetic moment of $0.2170\mu_B$. In the corresponding band structure illustrated in Fig. 10, we identify three partially filled two-dimensional bands that cross the Fermi level and sixteen full *d* bands. These bands accommodate 9 *d* electrons obtained by taking the average *d* charges per transition-metal ion and summing the charges of all the layers, as illustrated in Fig. 12 discussed below. The two majority spin partially filled bands and the single minority-spin partially filled band are responsible for the extra charge at V sites in layers 4 and 6 as shown in Fig. 9. The three full minority-spin bands, which are lower in energy than the partially filled minority-spin band but closer to the Fermi level than other full minority-spin bands, mainly contribute to

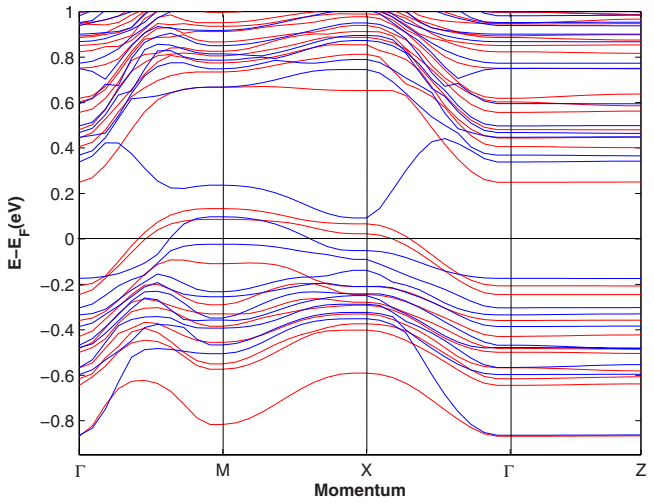

FIG. 10. (Color online) Spin-resolved band structure. The horizontal axis represents superlattice crystal momentum. The red solid lines represent the majority-spin bands, while the blue lines represent minority-spin bands. The momentum dependence along the layer direction k_z is captured in the region between the Γ and *Z* points. The three partially occupied bands associated with EIR are flat along k_z, demonstrating their quasi-two-dimensional character.

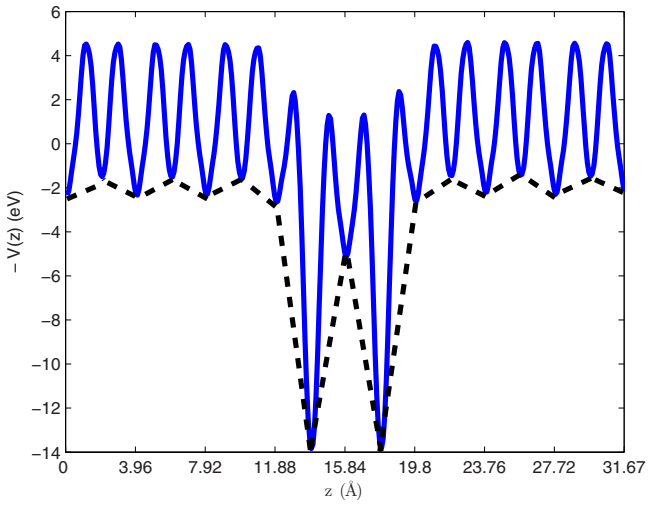

FIG. 11. (Color online) Plane-averaged Hartree potential along the layer-growth direction z. The solid dashed line indicates the net potential variation between charge-concentrated centers at each layer.

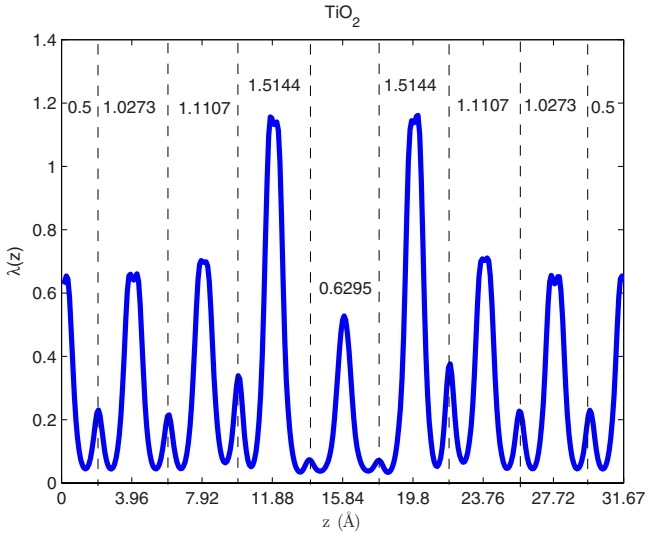

FIG. 12. (Color online) Linear electron number density $\lambda(z)$ along layer-growth direction z. The dashed lines represent the boundaries between different layers used in constructing the layer decomposition of this charge density. The numerical numbers between dashed lines in each layers are the total number of electrons from d-derivative bands in Fig. 10. In this case, the total number of electrons is nine.

minority-spin charge concentrated in layers 4, 5, and 6. The wave functions for those bands are strongly hybridized within those layers. The lowest majority-spin band in Fig. 10 is mainly of V character in layer 4 but lower in energy due to the more attractive local potential at this site. The peak of the DOS for the minority spin at the V site seems to shift higher toward the Fermi energy than expected. This is due to the fact those states are strongly hybridized with the states at the Ti sites which are shifted toward higher energy, an effect not included in the qualitative analysis. [See the potential profile of the realistic conjecture of case (b) in Fig. 1]. Other full bands are responsible for BVO bulk states away from the region in which the electronic interface reconstruction occurs.

In Fig. 11, we plot plane-averaged Hartree potentials. The first layer starts with VO_2 at $z=0$. Transition-metal layers repeat with a spatial period of 3.96 Å with the center ($z=15.84$ Å) layer occupied by TiO_2 layer. At $z=1.98$ Å, the first BaO layer starts and repeats also at a period of 3.96 Å; the local minima closest to TiO_2 correspond instead to LaO layers. By inspecting the local minima in the Hartree potential, we can see that the DFT calculations largely verify the scenario of case (b) in Fig. 1 except that the dashed line wiggles in the region of bulk BVO. The wiggling may be due to the slight difference of the strength of ionic bonding between Ba-O and V-O along the layer direction, which causes the small dipole modification of charge distribution in BVO ionized layers.

In Fig. 12, we show the corresponding electron linear number density $\lambda(z) \equiv 0.5 \int \rho(x,y,z) dxdy$ along the layer-growth direction. This charge number spatial distribution $\rho(x,y,z)$ include the total charges contributed from the bands between 0 and −0.9 eV with respect to Fermi level in Fig. 10. We see an apparent charge accumulation (1.5144 e^-) at the TiO_2 layers centered at $z=11.88$ Å and $z=19.8$ Å along with much less charge (0.6295 e^-) at the TiO_2 layer. Remote transition-metal layers have small deviations from a d^1 valence. The total amount of charges from the d-bands is 9 e^- by adding the charges at each layer in agreement with our prediction in case (b). The calculation shows small deviations from the ideal conjecture we made for this case and almost the realistic conjecture. In general, the charges in the well are transferred from the TiO_2 layer to adjacent VO_2 layers as discussed in Sec. II.

V. SUMMARY AND DISCUSSION

In this paper we have explored some possibilities for the realization of artificial two-dimensional electron systems by growing quantum wells consisting of a few atomic layers of one layered oxide surrounded by another material. In particular we consider systems that involve heterojunctions between polar insulating perovskites such as LTO and nonpolar insulating perovskites such as BVO. Perovskites can be viewed as consisting of alternating AO and BO_2 layers where B is a transition metal. The main idea of this paper is that inversion symmetric quantum wells will necessarily have a different number of AO and BO_2 layers and that this will necessarily lead to an electronic reconstruction which induces two-dimensional electron systems near the quantum well when one material is polar and one is nonpolar. Four different cases can be identified in which the quantum-well material is either polar or nonpolar and in which it either has an excess AO layer or an excess BO_2 layer. The excess layers induce either a unit increase or a unit decrease in the total d-orbital occupancy per transition-metal site when summed over all layers. This charge must be localized close to the quantum well to avoid large band shifts due to polarization-driven electrostatic potentials. As long as inversion symmetry around the quantum-well center is not broken spontaneously,

half of this charge must appear on each half of the quantum-well center. Because of the strong-correlation character of the oxide electronic structure, these charges will tend to be localized in half-filled LSDA+U bands which are weakly hybridized so that both cross the Fermi energy.

We have tested and elaborated on this qualitative picture of the electronic structure of polar-nonpolar heterojunction quantum wells in perovskites by performing self-consistent LSDA+U electronic structure calculations for a representative system composed of BVO and LTO without any atomic relaxation at the interface. The LSDA+U calculations capture the interplay between long-range polar electrostatic energy and local physics driven by energetic offsets between different transition-metal ions and by p-d hybridization. We find that in the two cases we have examined one additional two-dimensional bands is induced by the energetic offsets. In all cases the quantum-well structure creates a two-dimensional metal inside a three-dimensional Mott insulator and alters the character of the magnetic order. The reconstructed magnetic order is ferromagnetic in the active well region and antiferromagnetic in bulk region. The appearance of two-dimensional ferromagnetism in intimate exchange contact with antiferromagnetism is intriguing from the point of view of spintronics.

Because of the complexity of oxide materials, our calculation should be viewed as an exploration of possibilities rather than as predictive in any detailed sense. Among the many sources of uncertainty, the Hubbard U interaction used in our LSDA+U is a phenomenological parameter for which we have chosen standard bulk values. This value should likely be renormalized near the quantum well. More challenging to account for is the role of inevitable lattice distortions, oxygen stoichiometry variations, and other defects near the interfaces. The interfaces between the thin film oxide and the substrate on which it is grown can also play a complicating role if either the barrier material or the substrate is polar. For a few cases we have explored the influence of lattice distortion effects by allowing the atoms to relax along the layer-growth direction in the active region, maintaining $U_V = U_{Ti} = 3.2$ eV as before. What we do find is that the amount of charge transfer to or from particular layers and the details of the magnetic orders are highly sensitive to ionic relaxation. These complications make the accurate prediction of the electronic reconstruction and the associated magnetic order highly nontrivial. It is also desirable to understand if exotic symmetry breaking phases such as superconductivity may appear in the interface. We envision further progress in understanding detailed properties of the two-dimensional electron systems which almost certainly require inputs from experiments. The microscopic calculations reported here can be used as guidance in constructing phenomenological models which can be fit to any data which might emerge from future work and serve as the theoretical basis for possible exotic phases in the interface. The present paper has addressed d^1 transition-metal systems. Considerations similar to those explained here also apply to transition-metal oxides with heavy transition-metal elements (Cu and Ni) in which the t_{2g} bands are fully occupied far below the Fermi level and low-energy excitations are expressed within the e_g bands.

ACKNOWLEDGMENTS

This work was supported by the National Science Foundation under Grant No. DMR-0606489, by the Welch Foundation (Houston, TX) under Grants No. F-1473 and No. F-0934, by the Texas Advanced Computing Center (TACC), University of Texas at Austin. B.S. thanks SRC-NRI (SWAN) for financial support. C.-C.J.W. gratefully acknowledges helpful conversations with Peter Abbamonte.

*joseph@physics.utexas.edu

[1] P. A. Lee, N. Nagaosa, and X.-G. Wen, Rev. Mod. Phys. **78**, 17 (2006).
[2] A. P. Ramirez, J. Phys.: Condens. Matter **9**, 8171 (1997).
[3] M. Imada, A. Fujimori, and Y. Tokura, Rev. Mod. Phys. **70**, 1039 (1998).
[4] A. Ohtomo, D. A. Muller, J. L. Grazul, and H. Y. Hwang, Nature (London) **419**, 378 (2002); A. Ohtomo and H. Y. Hwang, *ibid.* **427**, 423 (2004); H. Y. Hwang, MRS Bull. **31**, 28 (2006); N. Nakagawa, H. Y. Hwang, and D. A. Muller, Nature Mater. **5**, 204 (2006).
[5] N. Reyren, S. Thiel, A. D. Caviglia, L. Fitting Kourkoutis, G. Hammerl, C. Richter, C. W. Schneider, T. Kopp, A.-S. Retschi, D. Jaccard, M. Gabay, D. A. Muller, J.-M. Triscone, and J. Mannhart, Science **317**, 1196 (2007).
[6] A. Brinkman, M. Huijben, M. Van Zalk, J. Huijben, U. Zeitler, J. C. Maan, W. G. Van der Wiel, G. Rijnders, D. H. A. Blank, and H. Hilgenkamp, Nature Mater. **6**, 493 (2007).
[7] C. H. Ahn, A. Bhattacharya, M. Di Ventra, J. N. Eckstein, C. Daniel Frisbie, M. E. Gershenson, A. M. Goldman, I. H. Inoue, J. Mannhart, Andrew J. Millis, Alberto F. Morpurgo, and Douglas Natelson, Rev. Mod. Phys. **78**, 1185 (2006).
[8] S. Okamoto, A. J. Millis, and N. A. Spaldin, Phys. Rev. Lett. **97**, 056802 (2006).
[9] Rossitza Pentcheva and Warren E. Pickett, Phys. Rev. Lett. **99**, 016802 (2007).
[10] W.-C. Lee and A. H. MacDonald, Phys. Rev. B **74**, 075106 (2006); **76**, 075339 (2007).
[11] S. Altieri, L. H. Tjeng, F. C. Voogt, T. Hibma, and G. A. Sawatzky, Phys. Rev. B **59**, R2517 (1999); J. van den Brink and G. A. Sawatzky, Europhys. Lett. **50**, 447 (2000).
[12] H.-S. Ahn, D. D. Guong, J. Lee, and S. Han, J. Korean Phys. Soc. **49**, 1536 (2006).
[13] M. Cwik, T. Lorenz, J. Baier, R. Müller, G. André, F. Bourée, F. Lichtenberg, A. Freimuth, R. Schmitz, E. Müller-Hartmann and M. Braden, Phys. Rev. B **68**, 060401(R) (2003).
[14] G. Kresse and J. Furthmüller, Phys. Rev. B **54**, 11169 (1996).
[15] G. Kresse and J. Furthmüller, Comput. Mater. Sci. **6**, 15 (1996).
[16] G. Kresse and D. Joubert, Phys. Rev. B **59**, 1758 (1999).
[17] G. Kresse and J. Hafner, Phys. Rev. B **47**, 558 (1993).
[18] S. L. Dudarev, G. A. Botton, S. Y. Savrasov, C. J. Humphreys, and A. P. Sutton, Phys. Rev. B **57**, 1505 (1998).
[19] M. T. Czyzyk and G. A. Sawatzky, Phys. Rev. B **49**, 14211 (1994).
[20] S. Okatov, A. Poteryaev, and A. Lichtenstein, Europhys. Lett. **70**, 499 (2005).